ISOMAse
International Society of Ocean, Mechanical and Aerospace Scientists and Engineers
Journal of Ocean, Mechanical and Aerospace
-Science and Engineering-
30th November 2025. Vol.69 No.3
DOI: 10.36842/jomase.v69i3.559

Multi-Parameter Vibration Analysis for Bearing Fault Detection at Low Speeds Using Standard Accelerometers with Stud and Magnetic Mounting

Noviandy [a] and Meifal Rusli [a,*]

[a)]*Mechanical Engineering Department, Faculty of Engineering, Universitas Andalas, Kampus Limau Manis, Padang - Indonesia*

*Corresponding author: meifal@eng.unand.ac.id

Paper History

Received: 12-October-2025
Received in revised form: 12-November-2025
Accepted: 30-November-2025

ABSTRACT

Detecting bearing defects at low rotational speeds remains a major challenge due to weak impulsive responses and dominant low-frequency components. This study evaluated the feasibility of using a standard industrial accelerometer (1 µA/ms², equivalent to 100 mV/g) for detecting outer race defects in bearings operating at 100–300 RPM. Experiments were conducted under both baseline and defected conditions using two mounting configurations: stud and magnetic. Vibration responses were analysed through overall values (velocity, acceleration, and shock pulse), spectral analysis, enveloped signals, and time waveform comparisons. Results show that standard accelerometers can effectively detect bearing defect signatures in low-speed machines (100–300 RPM), with diagnostic performance strongly influenced by the sensor mounting method. At 100 RPM, magnetic mounting occasionally recorded higher acceleration readings (≈30%) due to uneven impulsive energy distribution and low-speed dynamic instability. At higher speeds (200–300 RPM), stud mounting produced stronger and more stable responses, with amplitudes about 2–8% higher than magnetic mounting, confirming its superior coupling rigidity. Spectral analysis alone was limited by broadband noise, while time waveform and envelope analyses revealed clearer defect-related impacts, particularly at 1× RPM and 2× BPFO. Overall, stud-mounted sensors demonstrated more consistent and reliable performance, validating their suitability for accurate and practical low-speed vibration monitoring.

KEYWORDS: *Accelerometer, Bearing fault diagnosis, Low-speed rotation, Outer race defect, Vibration analysis.*

NOMENCLATURE

VSD	Variable Speed Drive
RPM	Rotation Per Minute
BPFO	Ball Pass Frequency Outer Race
BPFI	Ball Pass Frequency Inner Race
FFT	Fast Fourier Transform
DAQ	Data Acquisition System
EHL	Elastohydrodynamic Lubrication
RMS	Root Mean Square

1. INTRODUCTION

Early detection of bearing faults is essential for predictive maintenance, as it improves reliability, reduces costs, and prevents secondary damage. As highlighted by Weriono and Hendri [1], several types of damage that often occur in rotating machinery include faults in bearings, windings, and rotors, underscoring the critical role of bearing condition monitoring in maintaining overall system reliability.Vibration-based techniques such as envelope analysis and time waveform analysis have long been established as effective methods [2–6]. However, detecting such faults in low-speed machines (<300 RPM) remains a persistent challenge. At these speeds, the characteristic defect frequencies (BPFO, BPFI) typically occur below 10 Hz, and the resulting vibration amplitudes often fall below 0.1 g. Consequently, fault signatures are weak, easily masked by background noise, and often indiscernible in conventional frequency spectra [7–11].

Recent studies have explored several approaches to overcome these limitations. Researchers have emphasized the use of high-sensitivity accelerometers (>500 mV/g), narrow band-pass filtering, and advanced demodulation techniques to enhance weak impulsive responses under low signal-to-noise ratio (SNR) conditions [12–15]. Others have proposed time-domain impact analysis and shock pulse monitoring as complementary techniques to detect low-speed bearing defects where FFT-based methods may fail [16–20].

Despite their technical effectiveness, these advanced approaches often face practical limitations in real-world industrial environments. High-sensitivity accelerometers

are significantly more expensive, often five to ten times the cost of standard sensors, and tend to have lower durability, limited temperature tolerance, and higher susceptibility to electromagnetic interference. They frequently require low-noise signal conditioning systems, shielded cabling, or dedicated data acquisition hardware, which increases both installation complexity and maintenance cost. Similarly, specialized techniquessuch as acoustic emission or laser vibrometry, though highly sensitive, demand laboratory-grade setups and controlled environments, making them impractical for continuous on-site monitoring in factories or process plants.

These constraints create a clear gap between academic advancements and industrial feasibility, particularly for facilities seeking low-cost, scalable monitoring solutions.Similar field observations by Septano et al. [21] in coal crusher vibration analysis revealed increased axial vibration readings at the non-drive end (NDE) under load, indicating potential misalignment or bearing wear, further emphasizing the industrial relevance of cost-effective vibration-based diagnostics.

To address this gap, the present study investigates whether standard industrial accelerometers (1 µA/ms², equivalent to 100 mV/g), commonly used for routine vibration monitoring, can reliably detect outer race defects in bearings operating at 100–300 RPM. The study also compares two mounting configurations (stud vs. magnetic) to assess their influence on sensitivity and diagnostic performance.

This research specifically aims to:

1. Evaluate the capability of standardaccelerometers in detecting low-speed bearing defects.
2. Identify limitations related to signal sensitivity, resolution, and mounting configuration.
3. Assess the contribution of signal processing methods such as envelope and time waveform analysis in enhancing weak defect signatures; and
4. Provide practical recommendations for implementing cost-efficient condition monitoring strategies using standard, widely available sensors.

By integrating both a review of current research and controlled experimental validation, this study provides empirical evidence that standard accelerometers, when properly mounted and processed, offer a feasible and economical alternative for diagnosing bearing defects in low-speed rotating machinery.

2. METODOLOGY

2.1 Test Rig and Specification

This study utilizes an experimental rotor system (rotor kit) designed to simulate industrial machine operating conditions in a controlled environment. The system allows for variable rotational speeds, testing of various fault types, and flexible sensor placement at critical points.

The test setup consists of a three-phase induction motor controlled via a Variable Speed Drive (VSD) to regulate rotational speed. A solid steel shaft is mounted horizontally and supported by two bearing pedestals, each equipped with an accelerometer mounting point. The bearing type used is a Pillow Block Bearing Unit UCPH206, which incorporates an UC206 insert bearing (deep groove ball bearing, bore diameter 30 mm, outer diameter 62 mm). The UCPH206 in this setup contains 9 rolling elements (balls) with a diameter of approximately 10 mm, a pitch diameter of about 46 mm, and a contact angle of 0° (radial load). These parameters form the basis for calculating characteristic defect frequencies (BPFO, BPFI, BSF, and FTF).

The housing is a high-center pillow block type made of cast iron, grease-lubricated with a re-lubrication hole, and commonly used in light to medium industrial applications due to its durability and ease of installation. The sensor employed is a standard industrial accelerometer with a sensitivity of 1 µA/ms².Rotational speeds are set at three levels: 100 RPM, 200 RPM and 300 RPM, to represent the low-speed machine category (<300 RPM), as typically found in applications such as agitators, screw conveyors, and slow-speed rollers.The experimental setup, including the rotor kit and the mounted bearing UCPH206, is illustrated in Figure 1 to provide a clear visualization of the assembly and measurement configuration.

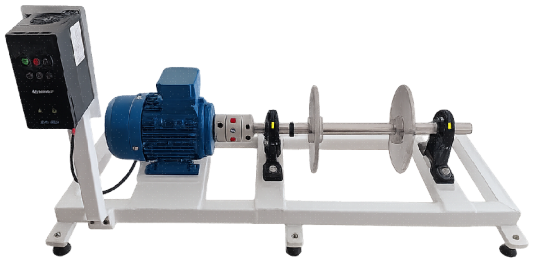

Figure 1: Rotor Kit and UCPH206 bearing used in the experimental setup

2.2 Fault Simulation

Two bearing conditions were evaluated: (1) baseline (healthy) and (2) outer race defected. The defect was artificially introduced via abrasion using a rotary grinder to form a small pit on the outer race, replicating surface fatigue damage. Artificially induced outer race defect on a UCPH206 bearing.can be seen in Figure 2.

Based on the bearing geometry, the theoretical Ball Pass Frequency Outer race (BPFO) values were 6.26 Hz (100 RPM), 11.94 Hz (200 RPM), and 18.12 Hz (300 RPM), serving as reference frequencies for identifying fault-related peaks in vibration spectra and envelope analysis.

Figure 2: Artificially induced defect on the outer race of UCPH206 bearing

JOMAse | Received: 12-October-2025 | Accepted: 30-November-2025 | [(69) 3: 229-239
Published by International Society of Ocean, Mechanical and Aerospace Scientists and Engineers, www.isomase.org., ISSN: 2354-7065 & e-ISSN: 2527-6085

2.3 Sensor and Data Acquisition

Vibration measurements were captured using the VIB 6.142R, a CLD (Current Line Drive) type accelerometer with a sensitivity of 1 μA/ms², equivalent in dynamic performance to a standard IEPE/ICP accelerometer (100 mV/g).

In this study, the term "standard-type accelerometer" refers to an industrially common, cost-effective vibration sensor typically used in routine condition monitoring, as opposed to specialized high-sensitivity accelerometers (500–1000 mV/g) that are significantly more expensive and require low-noise amplifiers. Standard-type sensors are widely available, rugged, and suitable for temperatures up to 120°C, making them representative of equipment used in general-purpose maintenance applications.

Sensors were installed using two mounting configurations, stud-mounted (rigid coupling via threaded adapter) and magnet-mounted (quick attachment using flat rare-earth magnets) (Figure 3). Both were positioned directly on the bearing housing near the load zone to ensure comparable vibration transmission paths.

Data were acquired using a dual-channel DAQ system integrated with spectral analysis software. Overall velocity (1–1000 Hz) and acceleration (1–10,000 Hz) values were measured with three averages per run for repeatability. Velocity spectra were recorded from 1–200 Hz (LOR = 3200), while acceleration spectra were measured from 1–400 Hz (LOR = 6400).

For high-frequency defect analysis, envelope detection was applied using band-pass filtering between 500 Hz and 10,000 Hz. To enhance reproducibility, detailed filter parameters are provided as follows:

- High-pass cut off: 500 Hz (to remove low-frequency machine noise)
- Low-pass cut off: 10,000 Hz (to isolate resonance region)
- H max (maximum envelope spectrum frequency): 400 Hz
- Line resolution: 4000 lines
- Averages: 3

Time waveform data were recorded with a sampling rate of 65,536 Hz and a record length of 2 seconds per condition, providing a frequency resolution better than 1 Hz. This ensured capture of both low-frequency rotational harmonics and high-frequency impulsive events.

2.4 Experimental Procedure

The rotor assembly was pre-balanced to minimize structural resonance and unwanted vibration. Tests were conducted at 100, 200, and 300 RPM for both bearing conditions (baseline and defected).For each test, measurements were taken sequentially using both mounting methods, stud and magnet, under identical boundary conditions.

2.5 Data Analysis Techniques

Six analytical techniques were employed to comprehensively assess vibration behavior:

1. Overall vibration analysis (velocity, acceleration, and shock pulse), for trend-based comparison of bearing health and mounting effects.
2. Frequency domain analysis (FFT), to identify 1X, BPFO, and harmonic content.

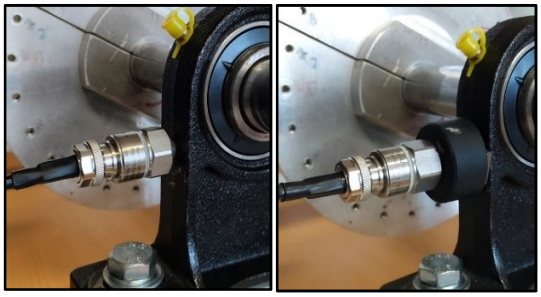

Figure 3: Mounting methods: stud (left) and magnet (right)

3. Shock pulse analysis, to quantify impact severity across speeds.
4. Time waveform analysis, to observe periodic impacts and modulation patterns.
5. Envelope analysis, using band-pass plus Hilbert transform to amplify weak defect responses.

2.6 Evaluation Result

Results were compared in terms of signal amplitude, fault identification accuracy, and consistency across speeds and mounting methods. This evaluation determined whether a standard-cost, medium-sensitivity accelerometer (1 μA/ms²) is sufficient for low-speed fault detection and quantified how envelope demodulation enhances weak impulsive signatures masked by broadband noise.

3. RESULT AND DISCUSSION

3.1 Overall Value Comparison

3.1.1 Overall Velocity

The measurement results of overall velocity indicate that sensor mounting significantly affects the sensitivity of bearing fault detection. When using a magnet mounting, vibration levels were relatively low, and little distinction was observed between the baseline bearing and the artificially defected bearing with an outer race defect. This suggests that magnet mounting is less effective in transmitting high-frequency vibration energy generated by the defect. In contrast, stud mounting revealed clearer differences, with the overall velocity of the defected bearing considerably higher than that of the baseline bearing, demonstrating its superior capability in capturing defect-induced vibrations.

Additionally, the results show a decreasing trend in overall velocity as rotational speed increases from 100 to 300 RPM. This can be attributed to the formation of thicker elastohydrodynamic lubrication (EHL) films at higher speeds, which reduce direct contact between the rolling elements and the outer race defect. Furthermore, increased kinetic momentum of the rolling elements at higher speeds causes impact energy to be more widely distributed, resulting in signal attenuation and lower recorded vibration responses. These findings suggest that bearing defect detection is more effective at lower speeds when using stud-mounted sensors. Comparative results of overall velocity measurements under both mounting methods across different rotational speeds are illustrated in Figure 4.

JOMAse | Received: 12-October-2025 | Accepted: 30-November-2025 | [(69) 3: 229-239
Published by International Society of Ocean, Mechanical and Aerospace Scientists and Engineers, www.isomase.org., ISSN: 2354-7065 & e-ISSN: 2527-6085

DOI:
10.36842/jomase.v69i3.559

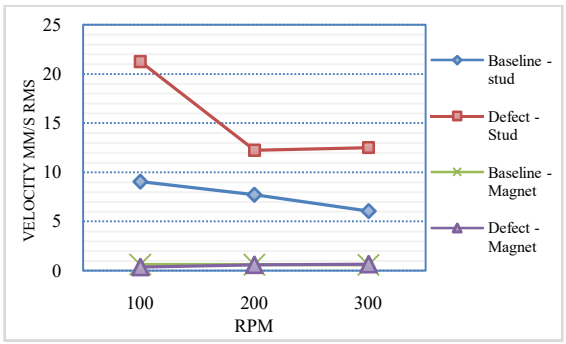

Figure 4: Overall velocity comparison between stud mounting and magnet mounting at 100, 200 and 300 RPM

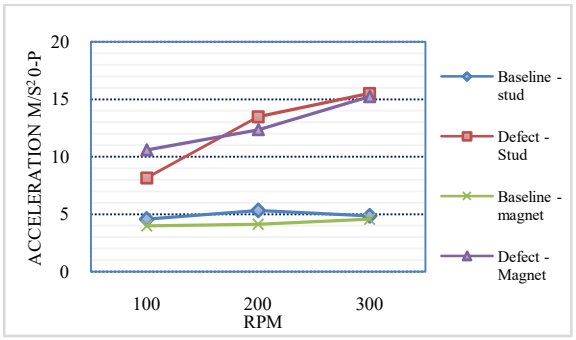

Figure 5: Overall acceleration comparison between stud mounting and magnet mounting for baseline and defected bearings at 100, 200, and 300 RPM

3.1.2 Overall Acceleration

A clearer illustration of these findings is presented in Figure 5, which compares the overall acceleration responses of both mounting methods at 100, 200, and 300 RPM under baseline and defected conditions. The plot highlights the anomalous case at 100 RPM, where the magnetic mounting produced unexpectedly higher amplitudes (≈30%)than the stud mounting, as well as the consistent trend reversal at higher speeds where the stud-mounted sensor exhibited superior sensitivity and stability (2–8% higher).

The overall acceleration measurements consistently show clear differences between normal (baseline) and defective bearings, with the defective bearing always exhibiting higher vibration levels. This confirms that the acceleration domain is highly sensitive to short-duration impulses generated by raceway defects. At 100 RPM, the acceleration of the defective bearing was nearly twice that of the normal bearing, although in this case, the magnet mounting recorded higher values than the stud mounting.

This anomaly at low speed (100 RPM) can be attributed to several interacting factors. First, at very low rotational speeds, the impulsive energy generated by rolling elements striking the defect is not evenly distributed over time, leading to non-periodic high-amplitude transients that may coincide with local resonance of the bearing housing or sensor mount. Second, the magnetic mount's partial compliance can cause micro-movements or tilting during these impacts, occasionally amplifying transient acceleration peaks in the recorded signal. Third, the magnetic base itself can slightly resonate with the bearing surface, particularly when the impact frequency lies near the natural frequency of the magnet–housing interface (typically around 1–2 kHz). This resonance produces sporadic amplitude spikes that are not representative of the actual bearing defect severity but rather of the mechanical coupling behaviour.

Additionally, because of the low speed, the number of impulsive events captured per time window is limited, and averaging may not fully suppress outlier peaks, causing higher variability in the magnet-mounted readings. The stud mounting, with its more rigid coupling, tends to produce a smoother and more repeatable response but may underrepresent single high-energy transients when impulsive energy is localized.

At 200 and 300 RPM, the measurements became more stable and consistent, with stud mounting generally producing higher overall acceleration values than magnet mounting. The more rigid coupling of stud mounting improves the sensor's sensitivity to high-frequency energy generated by periodic rolling element contacts with the defect, making defect-induced impulses more prominent at medium to high speeds.

Therefore, while the 100 RPM anomaly is explainable by low-speed dynamic instability, local resonance effects, and partial decoupling of the magnetic base, it also highlights the importance of considering mounting stiffness and transient response characteristics when interpreting low-speed vibration data. Overall acceleration remains an effective parameter for distinguishing between healthy and defective bearings, but results at very low speeds should be interpreted with caution, especially when using magnetic mounts.

3.1.3 Overall Shockpulse

The overall shock pulse comparison shows that magnet-mounted measurements are consistently lower than those obtained with stud mounting, confirming that stud mounting provides more rigid coupling and better transmission of high-frequency impulses generated by localized bearing defects. Across all tests, defected bearings produce higher shock pulse levels than baseline bearings, emphasizing the sensitivity of the method in distinguishing healthy and faulty conditions.

In addition, shock pulse levels exhibit a clear decreasing trend with increasing speed, which can be explained by overlapping impacts, the cushioning effect of a thicker elastohydrodynamic lubrication film, and broader energy distribution within the bearing structure. Despite these influences, stud-mounted sensors continue to capture defect impulses with higher clarity, underlining the importance of proper sensor mounting and accurate interpretation for reliable condition monitoring. The comparative results of overall shock pulse measurements under different mounting methods and bearing conditions at various speeds are presented in Figure 6.

3.2 Frequency Spectrum Comparison

3.2.1Velocity Spectrum Analysis

The velocity spectra comparison between the baseline and defected bearings shows that the vibration response is dominated by subsynchronous haystack-shaped broadband noise, with the 1×RPM component not clearly observable.

JOMAse | Received: 12-October-2025 | Accepted: 30-November-2025 | [(69) 3: 229-239
Published by International Society of Ocean, Mechanical and Aerospace Scientists and Engineers, www.isomase.org., ISSN: 2354-7065 & e-ISSN: 2527-6085

DOI:
10.36842/jomase.v69i3.559

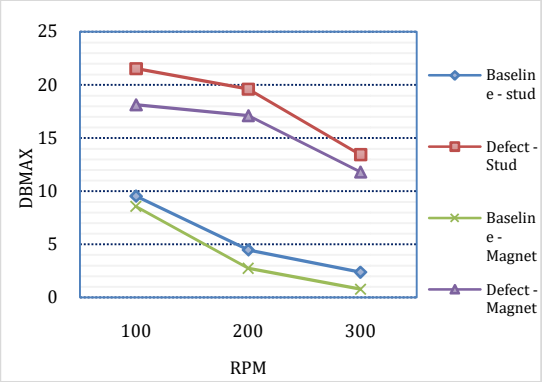

Figure 6: Overall shock pulse comparison between stud mounting and magnet mounting for baseline and defected bearings at 100, 200, and 300 RPM

Although the BPFO is present, its amplitude is very small (~0.08 mm/s RMS), making it difficult to detect bearing defects using only velocity spectra. This occurs because localized defects generate short-duration impacts with high-frequency energy, which are attenuated and spread into the subsynchronous noise in the velocity domain. At a rotational speed of 105.2 RPM, no distinct peak corresponding to the BPFO (6.25 Hz) is observed.

However, at 200.7 RPM, a clear BPFO peak appears at 12.12 Hz with an amplitude of 0.09 mm/s RMS, and at 304.7 RPM, the BPFO peak is detected at 18.5 Hz with an amplitude of 0.08 mm/s RMS. These frequencies were consistently observed in the data acquired using both stud and magnetic sensor mountings, confirming the presence of outer race fault signatures despite the masking effect of broadband noise.Figure 6 illustrates this behavior at 100 RPM with stud mounting, showing the baseline spectrum on top and the defected bearing spectrum below.

The figure 7 highlights that while both bearings exhibit similar broadband noise levels, the BPFO peak remains minor compared to the overall noise, indicating that acceleration or enveloping domains are more effective for identifying defect signatures.

The absence of a clear 1×RPM peak at 100–300 RPM is linked to small velocity amplitudes, masking by broadband noise, limitations of magnet mounting, and acquisition settings (Fmax, resolution, averaging). A recurring ~10 Hz peak may reflect either a structural resonance or a 2×RPM harmonic, which can be verified through run-up/coast-down tests or structural analysis.While velocity spectra are useful for identifying broadband responses and structural resonances, they are less effective for detecting localized bearing defects at low speeds.

3.2.2 Acceleration Spectrum Analysis

The acceleration spectra shows that the characteristic defect frequency, BPFO, is barely visible, with amplitudes of only 0.006–0.09 m/s² (0–P), making fault detection difficult using acceleration alone. At a rotational speed of 200.7 RPM, a BPFO peak is observed at 12.12 Hz with an amplitude of 0.006 m/s² (0–P) on stud mounting only, whereas at 304.7 RPM, a BPFO peak is detected at 18.31–18.5 Hz with an amplitude of 0.09 m/s² (0–P) on both stud and magnet mountings.

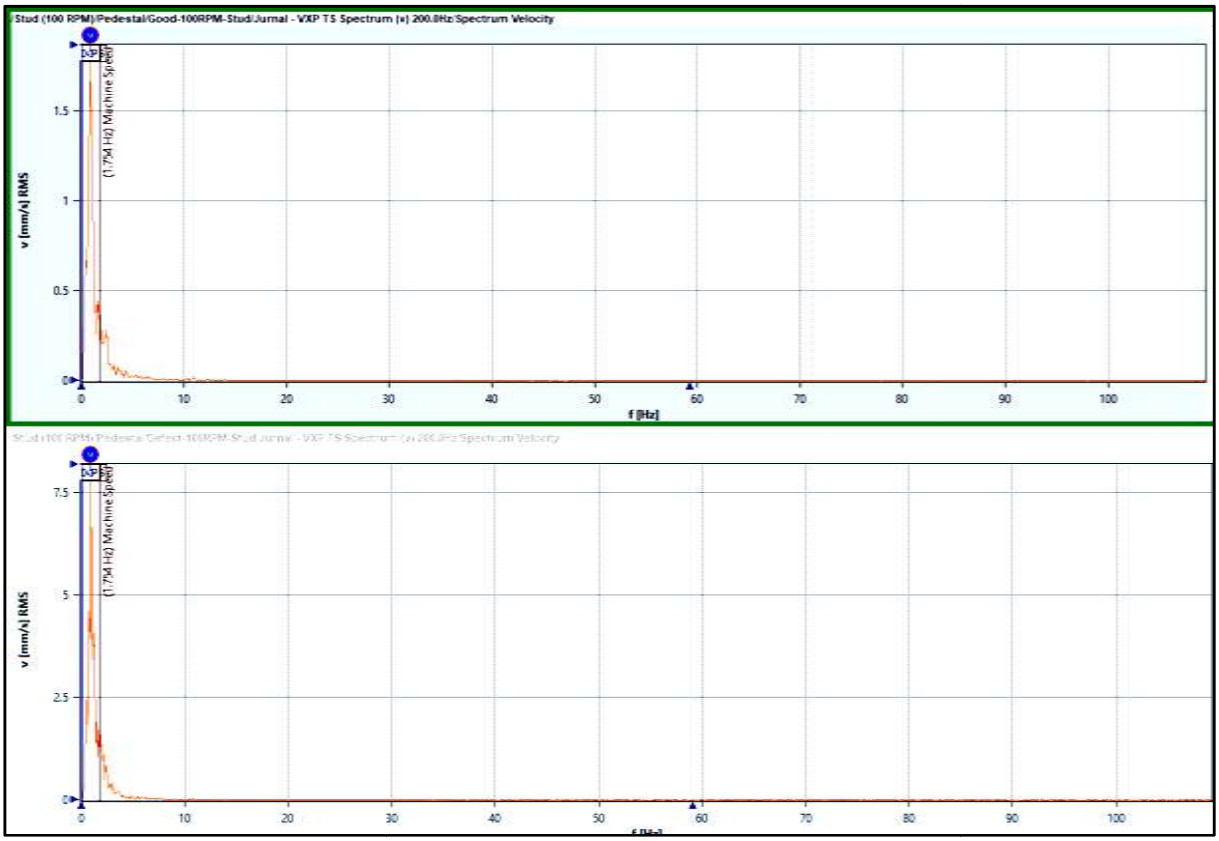

Figure 7: Velocity spectra at 100 RPM with stud mounting: baseline bearing (top) and defected bearing (bottom)

JOMAse | Received: 12-October-2025 | Accepted: 30-November-2025 | [(69) 3: 229-239
Published by International Society of Ocean, Mechanical and Aerospace Scientists and Engineers, www.isomase.org., ISSN: 2354-7065 & e-ISSN: 2527-6085

ISOMAse
International Society of Ocean, Mechanical and Aerospace Scientists and Engineers
Journal of Ocean, Mechanical and Aerospace
-Science and Engineering-
30th November 2025. Vol.69 No.3
DOI:
10.36842/jomase.v69i3.559

Instead, a rise in the noise floor and a haystack-shaped broadband response around 200 Hz dominates, reflecting the impulsive, short-duration nature of outer race defects that distribute energy into higher frequencies. This behavior can be observed in Figure 8, where the upper plot shows the baseline bearing and the lower plot shows the artificially defected bearing at 200 RPM using stud mounting.

These results indicate that while acceleration spectra reveal noise floor elevation and broadband features, they are insufficient for definitive fault diagnosis at low speeds.

3.2.3 Enveloping Spectrum Analysis

The enveloping spectra are dominated by strong 1×RPM harmonics from looseness or fit issues, which mask weaker outer race defect signals such as BPFO. These non-defect impacts reduce the sensitivity of envelope analysis. In fact, a BPFO peak is only observed at 304.7 RPM on stud mounting, appearing at 18.40 Hz with an amplitude of just 0.034 m/s² (0–P), while at other speeds and mounting conditions no distinct BPFO peaks can be identified. This indicates that although envelope analysis has potential for defect detection, its effectiveness in low-speed applications is limited when the defect signatures are extremely weak and heavily masked by structural or looseness-related components.

As shown in Figure 9, the envelope spectrum at 200 RPM with stud mounting did not clearly highlight the BPFO component. Both the baseline (upper plot) and defected bearing (lower plot) were dominated by shaft harmonics, particularly 4X, indicating structural looseness. These high-amplitude impacts masked the weaker fault-related signals, limiting the ability to isolate BPFO.

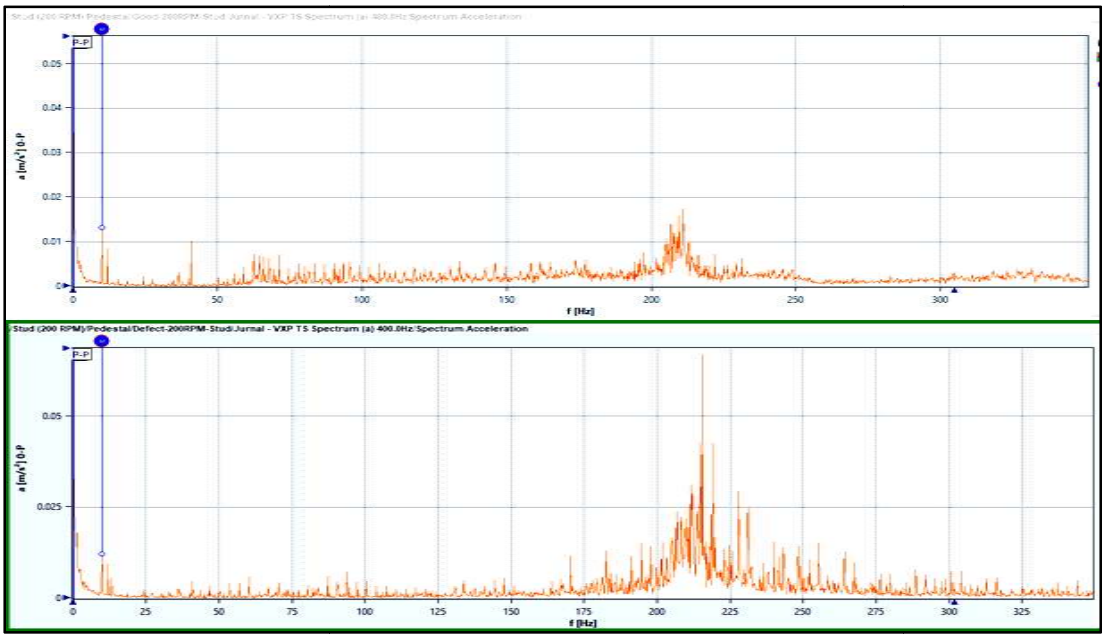

Figure 8: Acceleration spectra at 200 RPM with stud mounting: baseline bearing (top) and defected bearing (bottom)

Figure 9: Envelope spectra at 200 RPM with stud mounting: baseline bearing (top) and defected bearing (bottom)

JOMAse | Received: 12-October-2025 | Accepted: 30-November-2025 | [(69) 3: 229-239]
Published by International Society of Ocean, Mechanical and Aerospace Scientists and Engineers, www.isomase.org., ISSN: 2354-7065 & e-ISSN: 2527-6085

3.3 Time Waveform Analysis

3.3.1 Time Waveform Velocity Analysis

The velocity time waveform is dominated by low-frequency components, with no distinct impulsive peaks observed. This indicates that the signal primarily reflects the overall structural and rotational dynamics, rather than the localized impacts caused by bearing defects, making diagnosis based solely on velocity highly challenging.

These findings highlight the limitation of velocity-domain analysis for detecting outer race defects. While effective for identifying unbalance or misalignment, velocity lacks sensitivity to short-duration impulses. Figure 10 illustrates this at 100 RPM using stud mounting, where both baseline (upper plot) and defected bearing (lower plot) signals show dominant low-frequency content without clear impact peaks.

3.3.2 Time Waveform Acceleration Analysis

The time waveform acceleration data provides clearer insight into impulsive behavior than velocity signals, which are dominated by low-frequency components. For the baseline bearing, periodic impacts at 1X RPM appear across all speeds and mounting configurations, reflecting general machine dynamics rather than localized defects.

In contrast, the defected bearing shows stronger impulses, with 1X RPM impacts accompanied by peaks near 2X BPFO, caused by multiple rolling elements striking the defect within one shaft revolution. This highlights how defect geometry and load distribution can amplify higher harmonics. Overall, acceleration waveforms reveal defect-induced impulses more effectively than velocity, though the coexistence of 1X rotational impacts complicates interpretation. Figure 11 presents the acceleration waveforms at 100 RPM with stud mounting, showing the baseline bearing (upper plot) and defected bearing (lower plot).

3.3.3 Time Waveform Enveloping Analysis

The time waveform in the enveloping domain highlights impulsive features closely related to bearing defect frequencies, more effectively than raw velocity or acceleration signals. For the artificially defected outer race bearing, impacts occur at 1X shaft rotation, with additional peaks around 2X BPFO, particularly at 100 and 200 RPM, for both stud and magnet mounting. This demonstrates the ability of enveloping analysis to isolate defect-related periodicities from broadband vibration.

Figure 12 illustrates this at 200 RPM with stud mounting, showing the baseline bearing in the upper trace and the defected bearing in the lower trace, where peaks at 1X shaft revolution and 2X BPFO are clearly visible.

As a result, while the enveloped time waveform provides strong diagnostic potential at lower speeds by clearly revealing periodicities such as 2X BPFO, its effectiveness diminishes at higher speeds when impulsive signatures become masked by broadband excitation and dominant low-order harmonics. This finding emphasizes the importance of combining time waveform, spectrum, and advanced demodulation techniques to ensure reliable bearing fault detection across varying operational speeds.

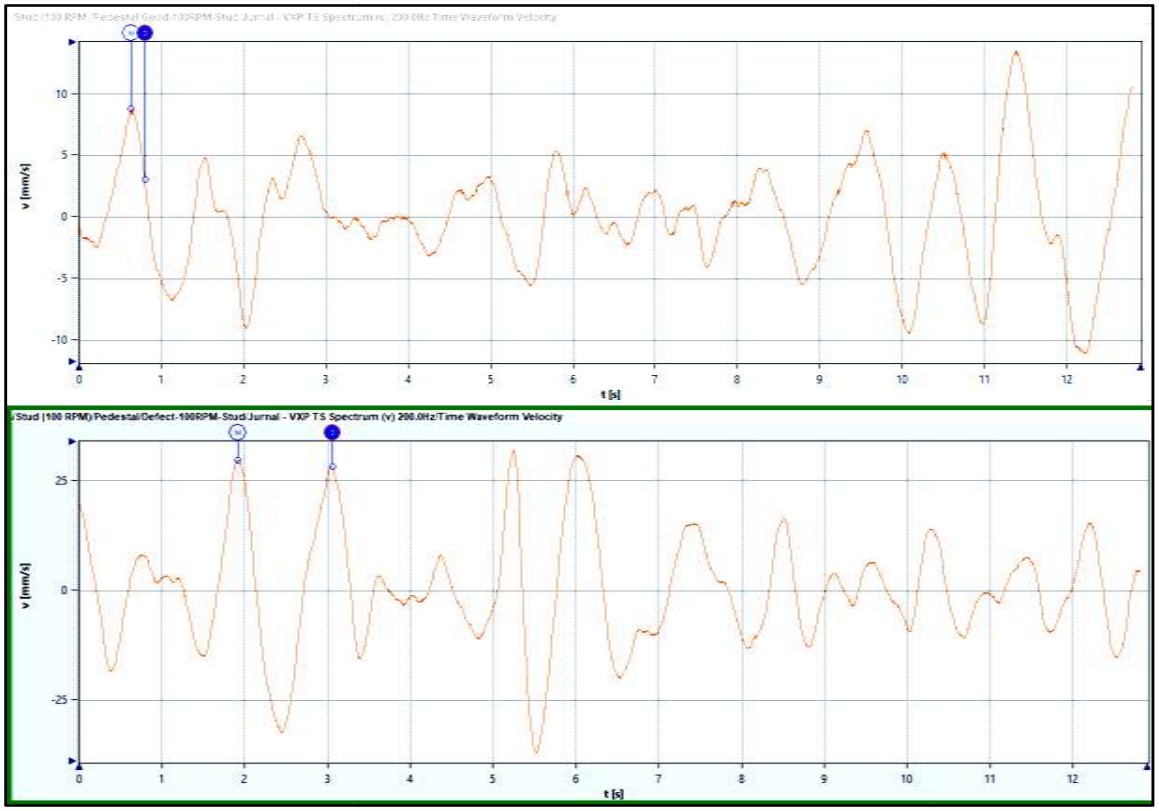

Figure 10: Time waveform in the velocity domain at 100 RPM with stud mounting. Upper plot: baseline bearing; lower plot: defected bearing

JOMAse | Received: 12-October-2025 | Accepted: 30-November-2025 | [(69) 3: 229-239]
Published by International Society of Ocean, Mechanical and Aerospace Scientists and Engineers, www.isomase.org., ISSN: 2354-7065 & e-ISSN: 2527-6085

DOI:
10.36842/jomase.v69i3.559

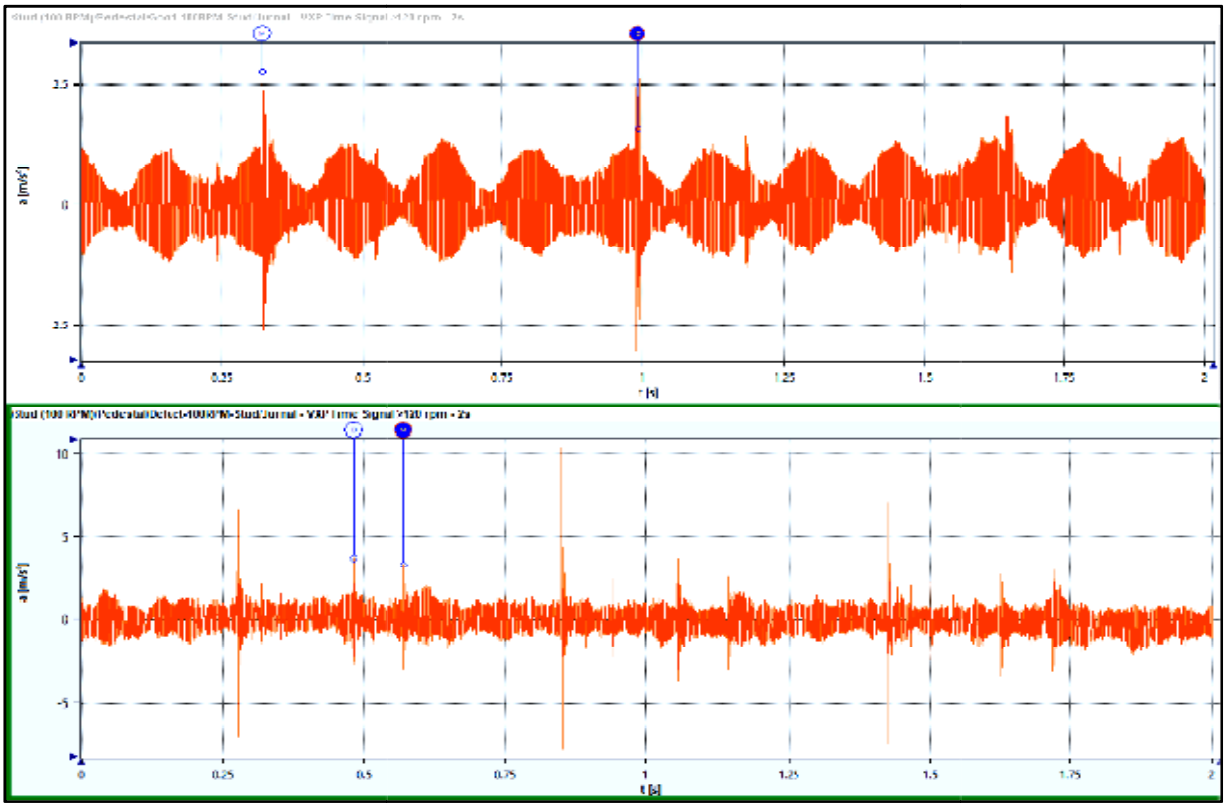

Figure 11: Time waveform acceleration at 100 RPM with stud mounting. Upper plot: baseline bearing; lower plot: defected bearing

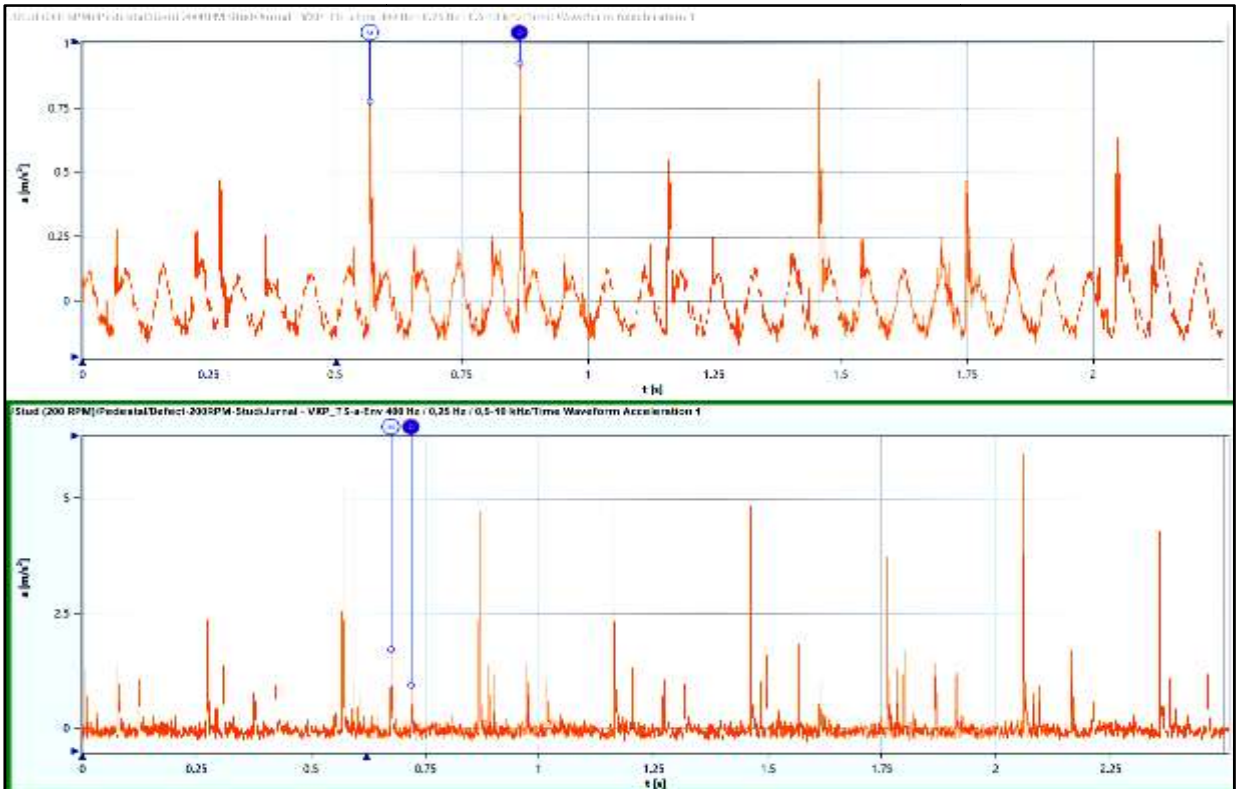

Figure 12: Time waveform enveloping at 200 RPM with stud mounting. Upper trace: baseline bearing; lower trace: defected bearing

JOMAse | Received: 12-October-2025 | Accepted: 30-November-2025 | [(69) 3: 229-239
Published by International Society of Ocean, Mechanical and Aerospace Scientists and Engineers, www.isomase.org., ISSN: 2354-7065 & e-ISSN: 2527-6085

3.4 Comparison of Stud and Magnet Mounting in Vibration Readings

In vibration monitoring, sensor mounting strongly affects data accuracy and reliability, influencing measured vibration amplitudes and machine condition assessment. This section systematically analyzes differences between stud-mounted and magnet-mounted sensors, examining velocity RMS, acceleration 0-P, and shock pulse across various speeds and bearing conditions. The discussion highlights how mounting choice impacts vibration readings and guides selection for reliable fault detection.

3.4.1 Overall Velocity RMS

The comparison between stud and magnet-mounted accelerometers shows that sensor mounting type significantly influences vibration amplitude measurements across all speeds (100, 200, and 300 RPM). Magnet mounting consistently recorded lower amplitudes, averaging 90–98% of the values obtained with stud mounting, which provides a more rigid and accurate coupling. This effect was observed for both baseline and defected bearings, with the influence more pronounced at lower speeds where mounting rigidity is critical for capturing defect-related impulses. The reduced fidelity of magnet mounting is linked to its less rigid attachment, which attenuates part of the vibration signal, while stud mounting ensures higher signal accuracy and diagnostic sensitivity. The percentage differences between mounting methods for both bearing conditions at different speeds are illustrated in Figure 13.

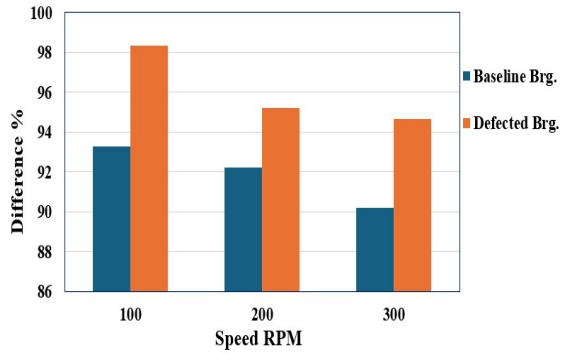

Figure 13: Percentage difference between stud and magnet mounting across 100, 200, and 300 RPM for baseline and defected bearings in velocity unit

3.4.2 Overall Acceleration 0-P

The comparison of peak-to-peak (0-P) acceleration measurements between stud and magnet mounting shows variable trends across different speeds and bearing conditions. Unlike velocity RMS, which remained relatively stable, acceleration 0-P measurements display inconsistencies, particularly at low rotational speeds.

At 100 RPM, the difference between stud and magnet mounting was 12.95% for the baseline bearing and -29.82% for the defected bearing. At 200 RPM, the discrepancies increased to 22.61% and 8.34%, respectively, while at 300 RPM, they decreased to 5.89% and 1.70%. The negative value at 100 RPM for the defected bearing suggests that the magnet-mounted sensor occasionally recorded higher peak-to-peak values, possibly due to local resonance effects or sensor positioning.

These results indicate that stud mounting provides more consistent and reliable acceleration measurements, especially at low speeds and for baseline bearings. Magnet mounting may be acceptable at medium and high speeds but can produce irregular or higher readings under certain low-speed defected conditions. Therefore, for accurate peak-to-peak acceleration monitoring and early fault detection, stud mounting is strongly recommended. Figure 14 illustrates the variations in measurements for both mounting types across speeds and bearing conditions.

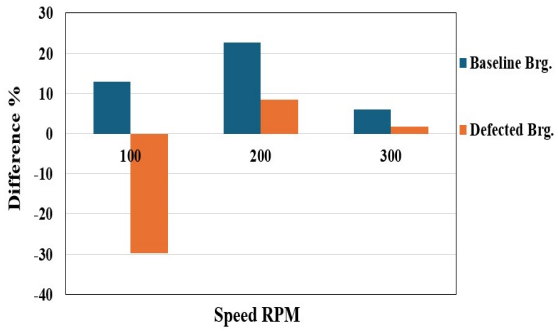

Figure 14: Percentage difference between stud and magnet mounting across 100, 200, and 300 RPM for baseline and defected bearings in velocity unit

3.4.3 Shock Pulsed Bmax

The comparison of shock pulse measurements between stud and magnet mounting shows clear differences depending on rotational speed and bearing condition, as illustrated in Figure 15. At 100 RPM, the percentage difference between the two mounting methods was 10.14% for the baseline bearing and 21.25% for the defected bearing. At 200 RPM, the discrepancy increased sharply to 38.81% for the baseline condition, while for the defected bearing it decreased to 10.73%. At 300 RPM, the difference for the baseline bearing reached the highest value of 67.61%, whereas the defected bearing condition remained comparatively low at 13.28%.

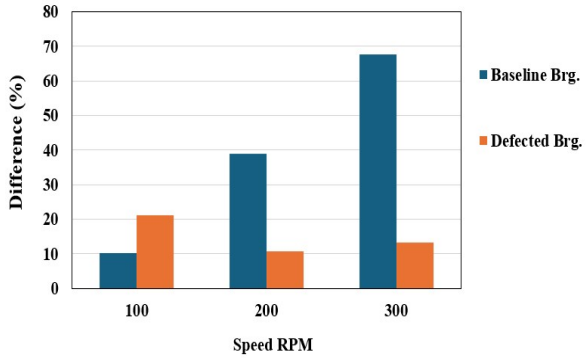

Figure 15: Percentage difference between stud and magnet mounting across 100, 200, and 300 RPM for baseline and defected bearings in shockpulse dB max

These results highlight two important trends. First, in the baseline condition, the discrepancy between stud and

JOMAse | Received: 12-October-2025 | Accepted: 30-November-2025 | [(69) 3: 229-239]
Published by International Society of Ocean, Mechanical and Aerospace Scientists and Engineers, www.isomase.org., ISSN: 2354-7065 & e-ISSN: 2527-6085

magnet mounting increases substantially with speed, indicating that magnet mounting is less effective at transmitting high-frequency shock impulses when no significant bearing damage is present. Second, under defected bearing conditions, the discrepancies are consistently lower, ranging from 10% to 21%, suggesting that strong defect-induced impulses can still be captured by magnet mounting, albeit with some amplitude loss.

Overall, stud mounting provides more reliable shock pulse measurements across all speeds and bearing conditions, particularly for baseline bearings at higher speeds where signal attenuation can exceed 60%. Figure 15 clearly demonstrates the superior performance of stud mounting in capturing both weak and strong impulse signals, making it the preferred choice for accurate shock pulse monitoring and early detection of bearing faults.

4. CONCLUSION

This study evaluated the capability of a standard accelerometer (1 µA/ms², equivalent to 100 mV/g) to detect bearing defects in low-speed machinery (100–300 RPM), considering different sensor mounting methods. The results confirm that standard accelerometers can capture bearing defect signatures even in the presence of additional machine faults such as looseness and fatigue. Overall vibration measurements, including velocity RMS, peak-to-peak acceleration (0–P), and shock pulse, reflected trends consistent with bearing degradation, but their diagnostic sensitivity strongly depended on the method of sensor mounting.

The overall acceleration data showed clear distinctions between healthy and defective bearings. At 100 RPM, an anomaly was observed where the defected bearing produced higher acceleration readings with magnet mounting than with stud mounting, likely due to uneven impulsive energy distribution, transient resonance of the magnetic base, and unstable low-speed response. At 200 and 300 RPM, stud mounting consistently provided higher and more stable overall acceleration, demonstrating the importance of rigid coupling for capturing high-frequency impulses generated by rolling element contacts with outer race defects. Velocity RMS measurements indicated that stud mounting consistently recorded 90–98% higher amplitudes than magnet mounting, especially at lower speeds, while shock pulse measurements confirmed that stud-mounted sensors captured defect impulses with greater clarity across all speeds.

Spectral analysis alone showed limited sensitivity to defect frequencies, often masked by broadband noise and structural harmonics. In contrast, time waveform acceleration and enveloped signals were more effective in revealing defect-induced impacts, particularly 1X RPM and 2X BPFO at 100–200 RPM. These features, however, tended to diminish at 300 RPM due to impact broadening, structural resonance, and the damping effect of thicker lubrication films. Hence, a combination of time waveform, envelope analysis, and spectral interpretation proved essential for reliable diagnosis across varying speed conditions.

Overall, stud-mounted sensors demonstrated superior capability in capturing defect-induced vibration signals across all parameters, particularly at medium to high speeds. While magnetic mounting may occasionally register strong transients under defected conditions, stud mounting offers greater consistency and diagnostic reliability by ensuring more rigid mechanical coupling and optimal transmission of impulsive energy. Therefore, for accurate vibration monitoring and early detection of outer race defects in low-speed machinery, stud-mounted standard accelerometers are strongly recommended—complemented by acceleration and enveloped time waveform analyses to enhance fault visibility.

Future research should explore the cost-effectiveness and practical integration of these techniques into existing industrial condition monitoring systems, particularly in environments where low-cost retrofitting is preferred over high-end instrumentation. In addition, further studies could investigate other types of bearing defects such as inner race, ball element, or cage faults, under similar low-speed conditions, as well as the influence of lubrication regimes, mounting stiffness, and housing resonance on diagnostic accuracy. Such investigations would broaden the applicability of standard accelerometers and strengthen their role as a viable, economical alternative for predictive maintenance in slow-rotating machinery.

ACKNOWLEDGEMENTS

The authors would like to express sincere gratitude to all parties who have provided support, both materially and intellectually, which enabled the completion of this research. Furthermore, deep respect and great appreciation are extended to all those involved in the research activities at the University of Andalas.

REFERENCES

[1] Rinaldi, W., & Hendri, H. (2025). Investigating the influence of time variation on electric motor vibration characteristics. *JOMAse*, 69(2), 163–167.
[2] Randall, R.B. (2011). *Vibration-based condition monitoring*: Wiley.
[3] Tandon, N., & Choudhury, A. (1999). A review of vibration and acoustic measurement methods for the detection of defects in rolling element bearings. *Tribology International*, 32(8), 469–480.
[4] International Organization for Standardization. (2015). Condition monitoring and diagnostics of machines — Vibration condition monitoring — Part 3: Guidelines for vibration diagnosis (ISO Standard No. 13373-3).https://cdn.standards.iteh.ai/samples/40840/1b24cf9678c241bdbdb4edef67ca32c2/ISO-13373-3-2015.pdf.
[5] McFadden, P.D., & Smith, J.D. (1984). Vibration monitoring of rolling element bearings by the high-frequency resonance technique—A review. *Tribology International*, 17(1), 3–10.
[6] Jardine, A.K.S., Lin, D., &Banjevic, D. (2006). A review on machinery diagnostics and prognostics implementing condition-based maintenance.

Mechanical Systems and Signal Processing, 20(7), 1483–1510.

[7] Mobius Institute. (2020). Practical vibration analysis [Training manual]. Mobius Institute.

[8] Bently Nevada. (2003). Rolling element bearing methodology application guide (Publication No. 164934). GE Energy. https://www.scribd.com/document/460007014/Rolling-Element-Bearing-Methodology-Application-Guide-164934-pdf.

[9] Harris, T.A., &Kotzalas, M.N. (2006). *Rolling bearing analysis*: CRC Press.

[10] Huang, Y., et al. (2023). Fault diagnosis of low-speed rolling bearing based on adaptive techniques. *Wind Energy*, 26(5), 471–485.

[11] Gruber, H., et al. (2024). Evaluation of a condition monitoring algorithm for early bearing failure detection. *Machines*, 12(2), 142.

[12] Qiu, H., Lee, J., Lin, J., & Yu, G. (2006). Wavelet filter-based weak signature detection method and its application on rolling element bearing prognostics. *Journal of Sound and Vibration*, 289(4–5), 1066–1090.

[13] PCB Piezotronics. (2005). Accelerometer selection considerations: Charge and ICP® integrated circuit piezoelectric [Technical Note TN-17]. https://www.pcb.com/contentstore/MktgContent/LinkedDocuments/Technotes/TN-17_VIB-0805.pdf.

[14] El-Thalji, I., &J antunen, E. (2015). A summary of fault modelling and predictive health monitoring of rolling element bearings. *Mechanical Systems and Signal Processing*, 60, 252–272.

[15] Fort, A., et al. (2023). A low-complexity rolling bearing diagnosis technique combining vibration and speed measurements. *Sensors*, 23(17), 7546.

[16] Randall, R.B., & Antoni, J. (2011). Rolling element bearing diagnostics—A tutorial. *Mechanical Systems and Signal Processing*, 25(2), 485–520.

[17] Smith, W.A., & Randall, R.B. (2015). Rolling element bearing diagnostics using the Case Western Reserve University data: A benchmark study. *Mechanical Systems and Signal Processing*, 64–65, 100–131.

[18] Wu, G., et al. (2022). A review on rolling bearing fault signal detection methods based on different sensors. *Sensors*, 22(21), 8349.

[19] Sun, B., et al. (2025). State-of-the-art detection and diagnosis methods for rolling bearing defects: A comprehensive review. *Applied Sciences*, 15(2), 1001.

[20] Hakim, M., et al. (2023). A systematic review of rolling bearing fault diagnoses. *Petroleum Science and Engineering*, 219, 111129.

[21] Septano, G.D., Ikbal, F., Fathoni, S., Bahri, S.S., &Putri, S.M.M. (2024). Detection of damage motor and coal crusher in power plant TanjungEnim 3 × 10 MW using vibration analysis. *JOMAse*, 68(3), 155–160. doi:10.36842/jomase.v68i3.378.